Choi *et al. Molecular Medicine* (2026) 32:155
https://doi.org/10.1186/s10020-026-01535-z

Molecular Medicine

RESEARCH Open Access

Oncolytic adenovirus co-expressing IL-12 and shVEGF potentiates immune checkpoint blockade for treatment of renal cell carcinoma: in vitro, organ-on-a-chip, and in vivo evaluation

Joongwon Choi[1†], Chae-Ok Yun[2,3,4,5†], Sejung Maeng[6], Yunlim Kim[7,8], Eunyoung Park[2], Ji Yi[2], Se Young Choi[6], In Ho Chang[6*] and A-Rum Yoon[2,3,4*]

Abstract

Renal cell carcinoma (RCC) has been known as highly malignant and resistant to standard therapy due to its immunosuppressive tumor microenvironment and aberrant VEGF-mediated angiogenesis. To overcome these therapeutic limitations, here we assessed the therapeutic efficacy of an oncolytic adenovirus (oAd) co-expressing Interleukin-12 (IL-12) and a short hairpin RNA against VEGF (shVEGF) in combination with immune checkpoint inhibitors (ICIs). The oAd/IL12/shVEGF induced RCC-specific cancer cell death in vitro and 3D bioprinted model, leading to greater anti-tumor effect compared with oAd-GMCSF. Furthermore, it potentiates anti-tumor efficacy in RCC orthotopic tumor model. The potent antitumor effect induced by combination of oAd/IL12/shVEGF with anti-PD1 was due to CD4 + or CD8 + T cell- or NK cell-mediated antitumor immune response and effective inhibition of tumor-associated neovascularization. Collectively, oAd/IL12/shVEGF can be a potent strategy to overcome current limitations in conventional RCC therapy by converting the cold tumor microenvironment to an inflamed state to sensitize refractory tumors to ICIs.

Graphical Abstract

Multifaceted antitumor effects of oAd/IL12/shVEGF combined with anti-PD1 therapy in renal cell carcinoma. The therapeutic efficacy of this combination strategy was evaluated using in vitro, 3D bioprinted, and in vivo RCC models. oAd/IL12/shVEGF induces virus-mediated oncolysis and the release of tumor antigens, while IL-12 promotes antitumor immune activation and shVEGF suppresses VEGF-mediated tumor angiogenesis. In combination with

†Joongwon Choi and Chae-Ok Yun contributed equally to this work.

*Correspondence:
In Ho Chang
caucih@cau.ac.kr
A-Rum Yoon
ayoon@hanyang.ac.kr

Full list of author information is available at the end of the article

© The Author(s) 2026. **Open Access** This article is licensed under a Creative Commons Attribution-NonCommercial-NoDerivatives 4.0 International License, which permits any non-commercial use, sharing, distribution and reproduction in any medium or format, as long as you give appropriate credit to the original author(s) and the source, provide a link to the Creative Commons licence, and indicate if you modified the licensed material. You do not have permission under this licence to share adapted material derived from this article or parts of it. The images or other third party material in this article are included in the article's Creative Commons licence, unless indicated otherwise in a credit line to the material. If material is not included in the article's Creative Commons licence and your intended use is not permitted by statutory regulation or exceeds the permitted use, you will need to obtain permission directly from the copyright holder. To view a copy of this licence, visit http://creativecommons.org/licenses/by-nc-nd/4.0/.

anti-PD1 immune checkpoint blockade, oAd/IL12/shVEGF enhances CTL, Th1, and NK cell-mediated antitumor immunity, leading to potent therapeutic efficacy in renal cell carcinoma models.

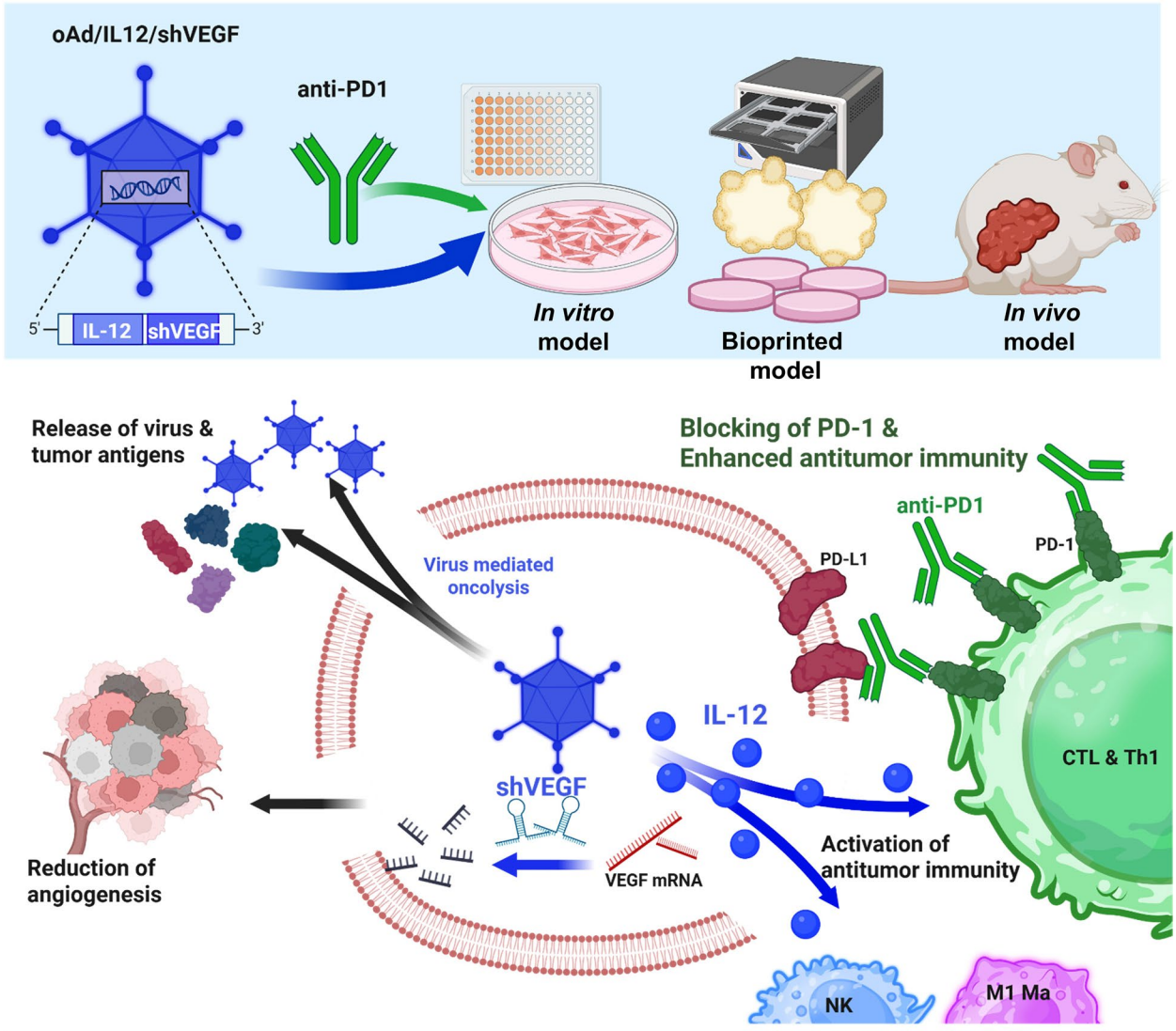

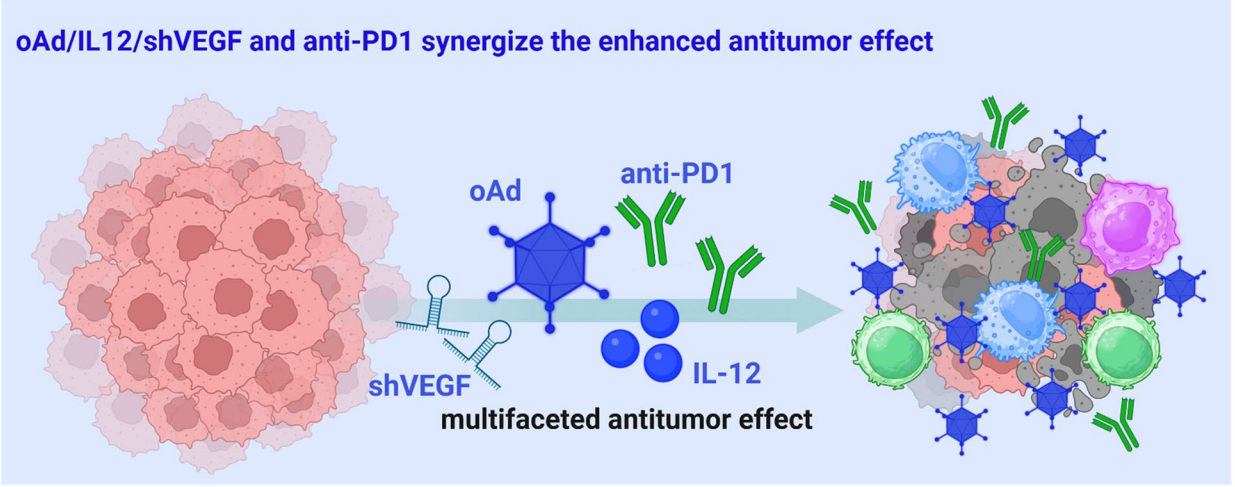

Key message

What is already known on this topic

RCC often acquires resistance against standard ICI due to its immunosuppressive cold microenvironment and VEGF-mediated abnormal angiogenesis.

What this study adds

Combining an oncolytic adenovirus expressing IL-12 and shVEGF (oAd/IL12/shVEGF) with anti-PD1 therapy transforms "cold" RCC into hot tumors by recruiting CD8+ T and NK cells while depleting regulatory T cells.

This combination therapy achieves superior synergistic antitumor efficacy and safety over monotherapies in both 3D-bioprinted and orthotopic mouse models through anti-tumor immune response.

How this study might affect research, practice or policy

The oAd/IL12/shVEGF platform offers a potent strategy to overcome immunotherapy resistance, potentially establishing a new clinical paradigm for treatment of patients with refractory RCC.

Introduction

Renal cell carcinoma (RCC) is a lethal malignant tumor with an increasing global incidence. Notably, approximately 25–30% of patients are already found to have metastatic RCC at diagnosis, and 30% of patients encounter recurrence even after surgical resection (Logan et al. 2012). Further, 5-year survival rate for metastatic RCC is less than 20%, highlighting the need for alternative treatment strategies. The clinical management of metastatic RCC has undergone a major transformation over the last three decades (Bedke et al. 2022). In the early 1990 s, treatment was centered on broad immune-activating cytokines like interleukin-2 and interferon-alpha (Coppin et al. 2005). While these therapies proved that RCC is responsive to immune modulation, they did not offer durable results and were associated with significant systemic toxicity (Motzer and Bukowski 2006). These nonspecific immune activation-caused safety concerns are a significant limitation to the practical application of cytokine-based treatments in clinical settings, necessitating a shift toward more precise therapeutic approaches with more manageable safety profiles.

The targeted drugs, such as tyrosine kinase inhibitors (TKIs) and mTOR inhibitors disrupting VHL/HIF/VEGF signaling axis, led a fundamental shift in mid-2000s for the treatment of patients with RCC (Motzer et al. 2007). However, these targeted therapies still have unmet needs due to resistance and recurrence for benefit of long-term patient survival. The development of ICIs, which precisely recalibrates the immune environment, has become a solution for unmet needs of previous cancer drugs and has moved again toward immuno-oncology (IO) combinations. The integration of immune checkpoint inhibitors (ICIs)—either as dual-agent therapy or alongside TKIs—now constitutes the standard, offering improved overall survival across multiple risk categories, significantly improving overall survival and durable response rates for patients (Amin and Hammers 2018).

RCC is known as a notably immunogenic malignancy. However, RCC often nullifies its immunogenicity by a coordinated immune escape factor (Jian et al. 2021). One of the key features of this contradiction is the overproduction of vascular endothelial growth factor (VEGF) by tumor cells with aberrant vessel proliferation (Wolf et al. 2023). This VEGF-regulated angiogenesis catalyzes tumor progression and compromises the host's immune surveillance by blocking the effective migration and metabolic activation of infiltrating T-lymphocytes. While ICIs have changed the therapeutic paradigm for metastatic RCC since late 2010, their objective responses remain 20–50% of the metastatic RCC patients (Young et al. 2024). This clinical resistance to treatment is frequently caused by paradoxical 'immunologically cold' microenvironment. Formation of aberrant vessels in tumor creates a biophysical signaling niche that favors RCC survival. Additionally, the structural instability of these vessels produces a localized hypoxic state, which decreased the effect of ICI treatment to trigger a robust anti-tumor response (Yang et al. 2024).

Based on our previous research, we hypothesized this oAd/IL12/shVEGF can be a powerful booster to maximize efficacy of ICI through a multiple mechanism of action (Graphical Abstract) (Yoon et al. 2023; 2019). 1) The oncolytic adenovirus can trigger direct tumor lysis and release of tumor-associated antigens and danger signals. These can lead to robust innate and adaptive immunity. 2) The therapeutic payload IL12 can be localized directly into the tumor site along with tumor specific viral replication. This targeted overcomes the systemic toxicity associated with traditional cytokine therapies (Qian et al. 2025) while changing the microenvironment toward an inflamed (Yoon et al. 2023; Liu et al. 2011). Further, genetic engineering techniques enable the incorporation the interleukin-12 (IL-12), which promotes natural killer (NK) cell activation and cytotoxic T lymphocyte (CTL) expansion. Which sequentially increases interferon-γ production and antigen presentation within the tumor microenvironment. 3) The other therapeutic gene shVEGF can not only reduce angiogenesis but also normalizes the abnormal blood vessel, thus facilitating the infiltration of activated T cells within the tumor tissue and restoration of immune mechanism to malignancy (Liu et al. 2025). 4) Through these mechanisms (antigen release, immune cell activation, and enhanced infiltration), the oAd can significantly increase the efficacy of ICI agents, even in cases resistant to standard treatment

(Ahn et al. 2025; Cheng et al. 2025). Collectively, work in concert to significantly amplify the efficacy of ICI agents, potentially overcoming resistance even in cases refractory to standard treatments.

Result

oAd/IL12/shVEGF expresses therapeutic genes and elicits RCC-specific cell killing effect

To address the dual challenge of angiogenesis and immune suppression in tumor cells in RCC, oAd encoding IL12 and shRNA targeting VEGF (oAd/IL12/shVEGF) has been utilized (Fig. 1A). The differences of viral production was not observed between group (control oAd vs oAd/IL12/shVEGF), showing that therapeutic gene did not hinder capability of virus to produce progeny virus (Fig. S1). As shown in Fig. 1B and Fig. S2, infection of human RCC cell line and murine RCC cell line with oAd/IL12/shVEGF led to a dose-dependent expression of IL12. The reduction of VEGF levels was observed in Renca cells, but not in A498 cells which is consistent with the mouse sequence-specific targeting of shVEGF. These results indicate that oAd/IL12/shVEGF was successfully constructed and functionally validated. The infection of human or murine RCC cancer cell lines with

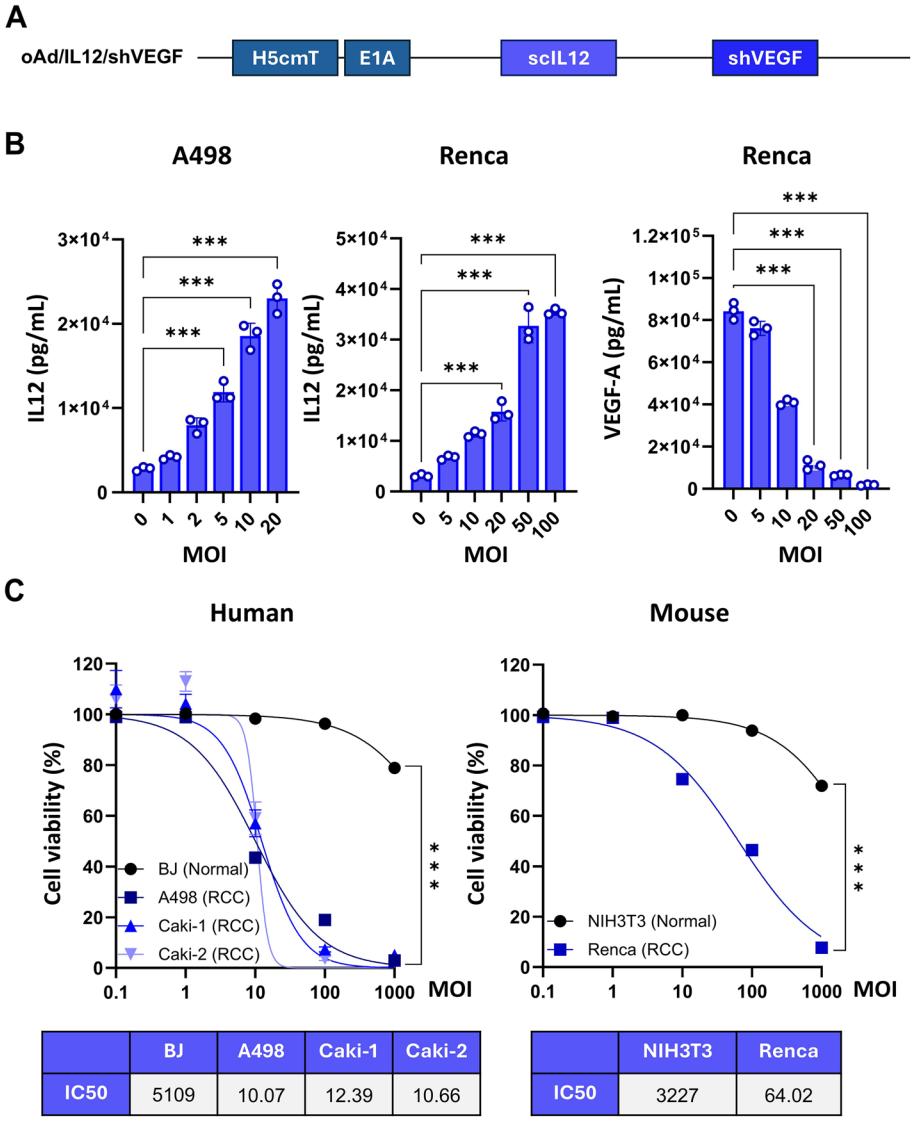

	BJ	A498	Caki-1	Caki-2
IC50	5109	10.07	12.39	10.66

	NIH3T3	Renca
IC50	3227	64.02

Fig. 1 Construction and in vitro characterization of oAd/IL12/shVEGF. **A** Schematic representation of the oncolytic adenovirus (oAd) genome used in this study: oAd/IL12/shVEGF. **B** Quantification for expression of Interleukin 12 (IL12) or VEGF-A by ELISA. Supernatants from A498 or Renca infected with the oAd/IL12/shVEGF were harvested and analyzed for IL12 or VEGF-A. **C** Cell viability assay of oAd/IL12/shVEGF-treated human renal cancer cell lines (A498, Caki-1, Caki-2), human fibroblasts (BJ), murine renal cancer cell lines (Renca), and murine fibroblasts (NIH3T3) at 48 h after infection. Data in **B** and **C** are presented as mean ± SD of triplicate wells and are representative of at least two independent experiments. Statistical significance was determined by one-way ANOVA followed by Tukey's multiple-comparisons test; *** $P < 0.001$

oAd/IL12/shVEGF led to dose-dependent cancer cell killing effect that was significantly more potent than that observed in normal cell lines (Fig. 1C; *** $P < 0.001$). oAd/IL12/shVEGF did not exert off-target cytopathic effect in murine or human fibroblast cell lines up to 100 multiplicity of infection (MOI), respectively. The shRNA encoded in oAd/IL12/shVEGF specifically targets murine VEGF sequences. Consequently, the reduction of VEGF levels was verified in murine RCC cell lines (Renca), confirming the mouse sequence-specific targeting of shVEGF. While the therapeutic effects observed in human tumor models (such as A498) are primarily attributed to oncolytic activity and IL12 expression, the Renca model demonstrates the additional functional benefit of VEGF suppression within a sequence-compatible context. Together, these results demonstrate that therapeutic genes expressed by oAd/IL12/shVEGF enhanced RCC killing effect with no observable off-target activity in normal cell lines.

oAd/IL12/shVEGF exerts selective cytotoxicity in a 3D bioprinted RCC model

To evaluate the therapeutic potential of oAd/IL12/shVEGF in a more complex architecture mimicking the tumor microenvironment, we utilized a 3D bioprinted model incorporating human umbilical vein endothelial cells (HUVEC), human foreskin fibroblasts (BJ), and A498 cell lines (Choi et al. 2023). As shown in Fig. 2, the structural integrity of the bioprinted lattice was monitored via Live/Dead staining. In the oAd/IL12/shVEGF-treated groups, a dose-dependent increase in red fluorescence (EthD-1, indicating dead cells) was observed specifically within the cancer cell-laden areas, while the viability of normal cell lines (BJ) remained relatively stable. Notably, viability of HUVEC cell lines decreased in a dose-dependent manner, due to anti-angiogenic properties of oAd/IL12/shVEGF. Quantitative analysis of A498 cell viability demonstrated that the cancer killing effect was further enhanced at 3 days post-infection compared to 1 day, with the highest dose 1×10^{10} viral particles (VP) showing a significant reduction in cell survival. Even though murine sequence specific shVEGF was expressed in human A498 3D model, this therapeutic efficacy can be driven by synergistic mechanisms such as high cross-reactivity of murine IL12 and E1A-mediated VEGF suppression. These results indicate that oAd/IL12/shVEGF can effectively penetrate 3D printed structures and selectively eliminate RCC cells without inducing significant off-target effects in the surrounding normal stroma.

oAd/IL12/shVEGF induces potent anti-tumor effect against subcutaneous RCC tumor model

To evaluate the antitumor efficacy of oAd/IL12/shVEGF, mice bearing subcutaneous A498 tumors were intratumorally treated with 1×10^6, 1×10^7 or 1×10^8 VP of oAd/IL12/shVEGF on day 0, 2, and 4 along with PBS as negative control (Fig. S3). The oAd/IL12/shVEGF showed tumor growth inhibition in a dose-dependent manner. In the subsequent experiment, therapeutic efficacy of oAd/IL12/shVEGF was compared with oAd-GMCSF. To ensure a rigorous comparison within the oAd platform, the control vector, oAd-GMCSF, was specifically designed as an analogue to ONCOS-102 (currently in clinical trials). This control oAd utilizes an Ad5/3 chimeric backbone where viral replication is strictly governed by a modified E1 region, featuring an E2F-driven E1A promoter in conjunction with a 24-base-pair deletion (Delta24) in the Rb-binding domain, while expressing human GMCSF. As shown in Fig. 3, PBS-treated group exhibited rapid tumor growth and reached an average tumor volume of 1386.53 ± 171.02 mm^3 on day 21 after the initial treatment. In contrast, both oAd/IL12/shVEGF and oAd-GMCSF induced significant tumor growth inhibition compared to PBS treatment group (** $P < 0.01$, * $P < 0.05$). oAd/IL12/shVEGF showed 3.6-fold increased anti-tumor effect than oAd expressing GMCSF. These results demonstrate that oAd/IL12/shVEGF underscores its clinical possibilities and supports further investigation in human clinical trials.

Synergistic antitumor effect of oAd/IL12/shVEGF in combination with anti-PD1

To evaluate the synergistic anti-tumor potential of oAd/IL12/shVEGF in combination with anti-PD-1 within a complex immune context, we utilized a 3D bioprinted RCC model incorporating Jurkat T cells and THP-1-derived macrophages to mimic the immunosuppressive tumor microenvironment. As shown in Fig. 4A, the presence of these immune cells explains the moderate cytotoxicity observed in the oAd/IL12/shVEGF or anti-PD-1 monotherapy group, as PD-1 blockade partially restores the effector function of immune cells against PD-L1-expressing RCC cells within the scaffold. More importantly, the combination group exhibited a markedly increased cancer-killing effect, indicating that oAd/IL12/shVEGF can enhance the multi-step therapeutic process. oAd-mediated IL-12 expression promotes the functional activation of both T cells and macrophages, while shVEGF-mediated.

suppression of VEGF reduces the immunosuppressive barrier of the TME. This suggests that oAd/IL12/shVEGF acts as a potent immune primer. We further assessed the effect of these treatments on T cell migration, a key factor in immune cell recruitment and therapeutic infiltration. The assay (Fig. 4B) revealed that the combination therapy significantly increased the T cell migration rate (area) compared to the control and monotherapy groups. These results demonstrate that oAd/IL12/shVEGF can act synergistically with anti-PD-1 to overcome the tumor

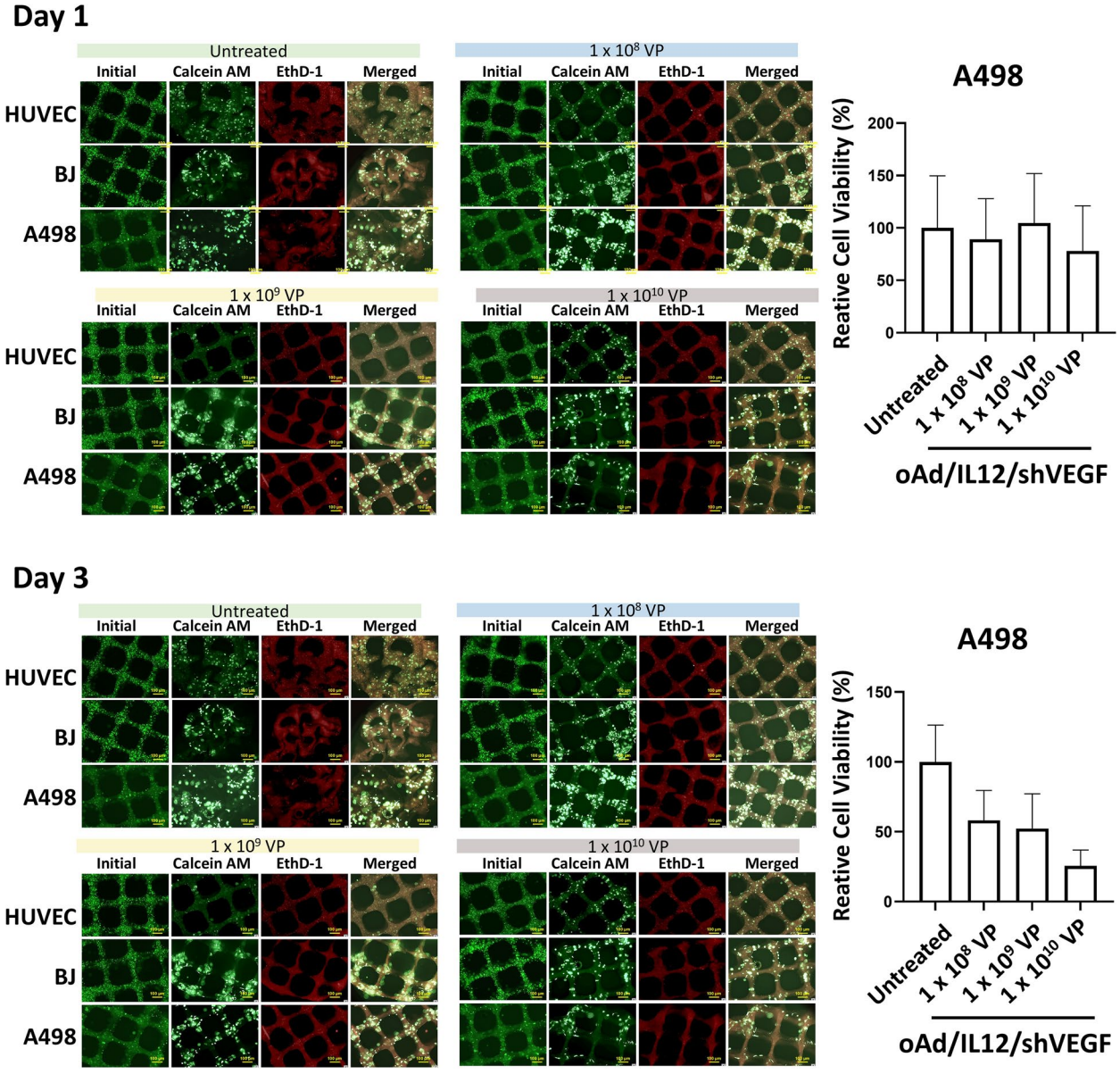

Fig. 2 Selective cell killing effect of oAd/IL12/shVEGF in a 3D bioprinted tumor model. **A** Representative fluorescence images of 3D bioprinted structures consisting of HUVEC, BJ, and A498 cells. The samples were treated with indicated concentrations of oAd/IL12/shVEGF (1×10^8 to 1×10^{10} VP) and stained with Calcein AM (green, live cells) and EthD-1 (red, dead cells) at 1 day and 3 days post-treatment (50× magnification). **B** Quantitative analysis of A498 cell viability in the 3D model at 1 day (1D) and 3 days (3D) post-infection. Cell viability was normalized to the untreated control group. Data are expressed as mean ± SD

microenvironment and maximize anti- tumor efficacy by promoting T cell infiltration into the tumor core.

Combined oAd/IL12/shVEGF with anti-PD1 significantly potentiates antitumor effect in tumor model

To evaluate the anti-tumor efficacy on combination of oAd/IL12/shVEGF with anti-PD1, subcutaneous Renca tumors were treated with oAd/IL12/shVEGF, anti-PD1, or oAd/IL12/shVEGF + anti-PD1, along with PBS as negative control (Fig. S4). PBS-treated groups exhibited rapid growth up to 20 days after the initial treatment. In contrast, anti-PD1 and oAd/IL12/shVEGF induced 42.1% and 51.5% inhibition of tumor growth, respectively. oAd/IL12/shVEGF + anti-PD1 treatments induced most potent antitumor effect compared with either anti-PD1 or oAd/IL12/shVEGF monotherapy, showing 72.6% and 67.2% superior tumor burden reduction, respectively, suggesting that combination of oAd/IL12/shVEGF and anti-PD1 can effectively control the growth of both in a safe manner.

To evaluate the in vivo therapeutic efficacy in a clinically relevant setting, we established an orthotopic RCC

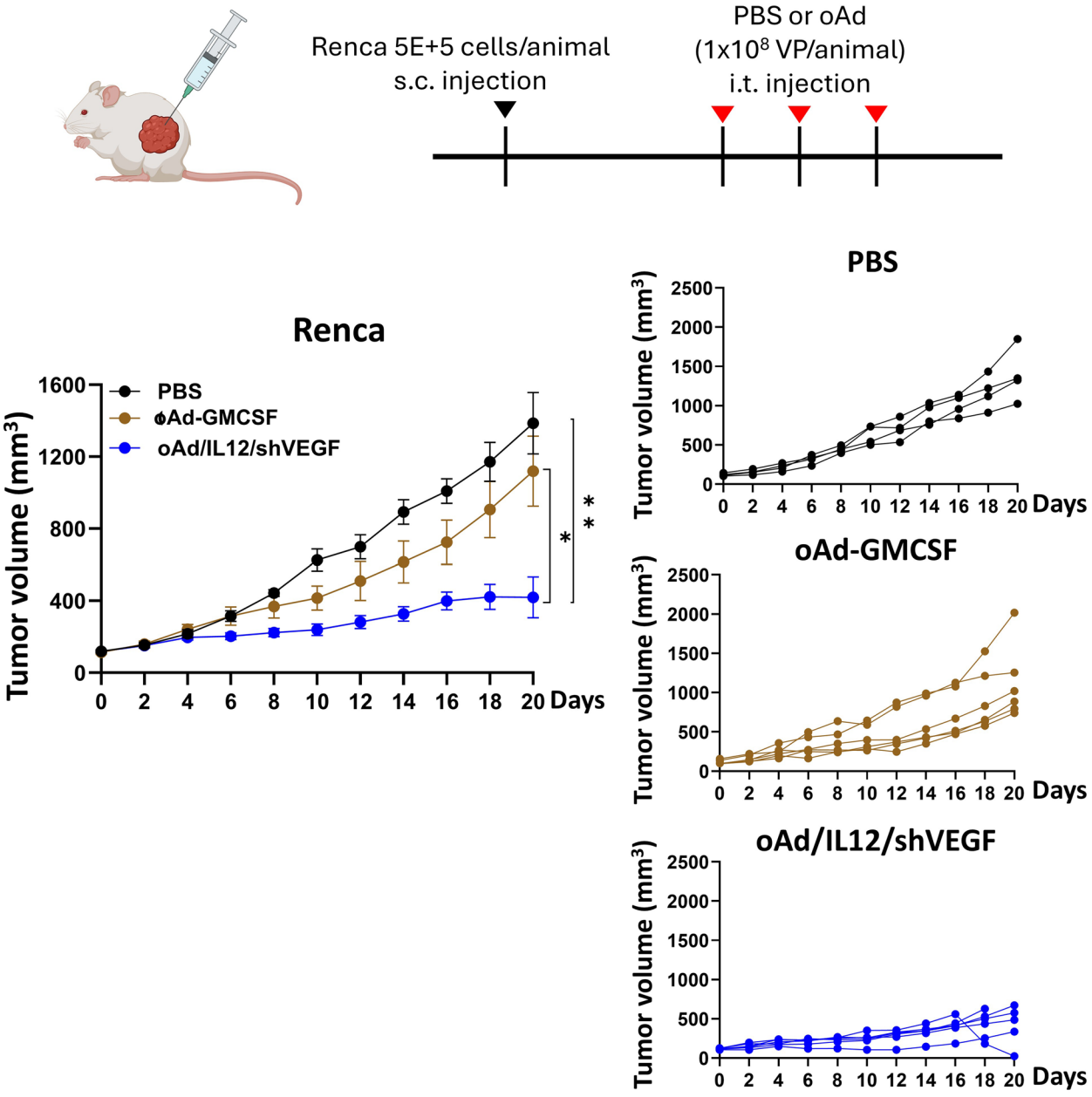

Fig. 3 Dose-dependent anti-tumor effect of oAd/IL12/shVEGF in Renca tumor model. **A** Renca cells were inoculated subcutaneously. When tumors reached approximately 100 mm^3, mice were treated by intratumoral (i.t.) injection with PBS, oAd-GMCSF, or oAd/IL12/shVEGF (1×10^8 VP). Dosing was performed 3 times every other day. Tumor volumes were monitored every 2 days. Left, mean tumor volume over time. Data are presented as mean ± SEM. Right, individual tumor growth curves for each group. Statistical significance across time and treatment groups was assessed by two-way ANOVA (time x treatment) followed by Tukey's multiple-comparisons test; $^*P < 0.05$, $^{**}P < 0.01$

model by injecting Renca-luc cells (5 $X10^5$ cells/50 µL) into the subcapsular space of the right kidney. As shown in Fig. 5A, tumor progression was monitored via bioluminescence imaging (BLI) at 5, 8, 13, and 15 days post-implantation. While the control group showed rapid tumor growth as indicated by increasing luciferase signal intensity, the group treated with the combination of oAd/IL12/shVEGF and anti-PD1 exhibited the most potent suppression of tumor bioluminescence. Quantitative analysis of the region of interest (ROI) signals (Fig. 5B) confirmed that the combination therapy significantly outperformed both the monotherapy and control groups at the final point (Day 15). Additionally, to assess systemic toxicity, mouse body weights were recorded throughout the 15-day period. As shown in Fig. 5C, even though decrease in body weight was observed in all groups including the control, histopathological analysis of the liver and spleen in the oAd/IL12/shVEGF-treated group

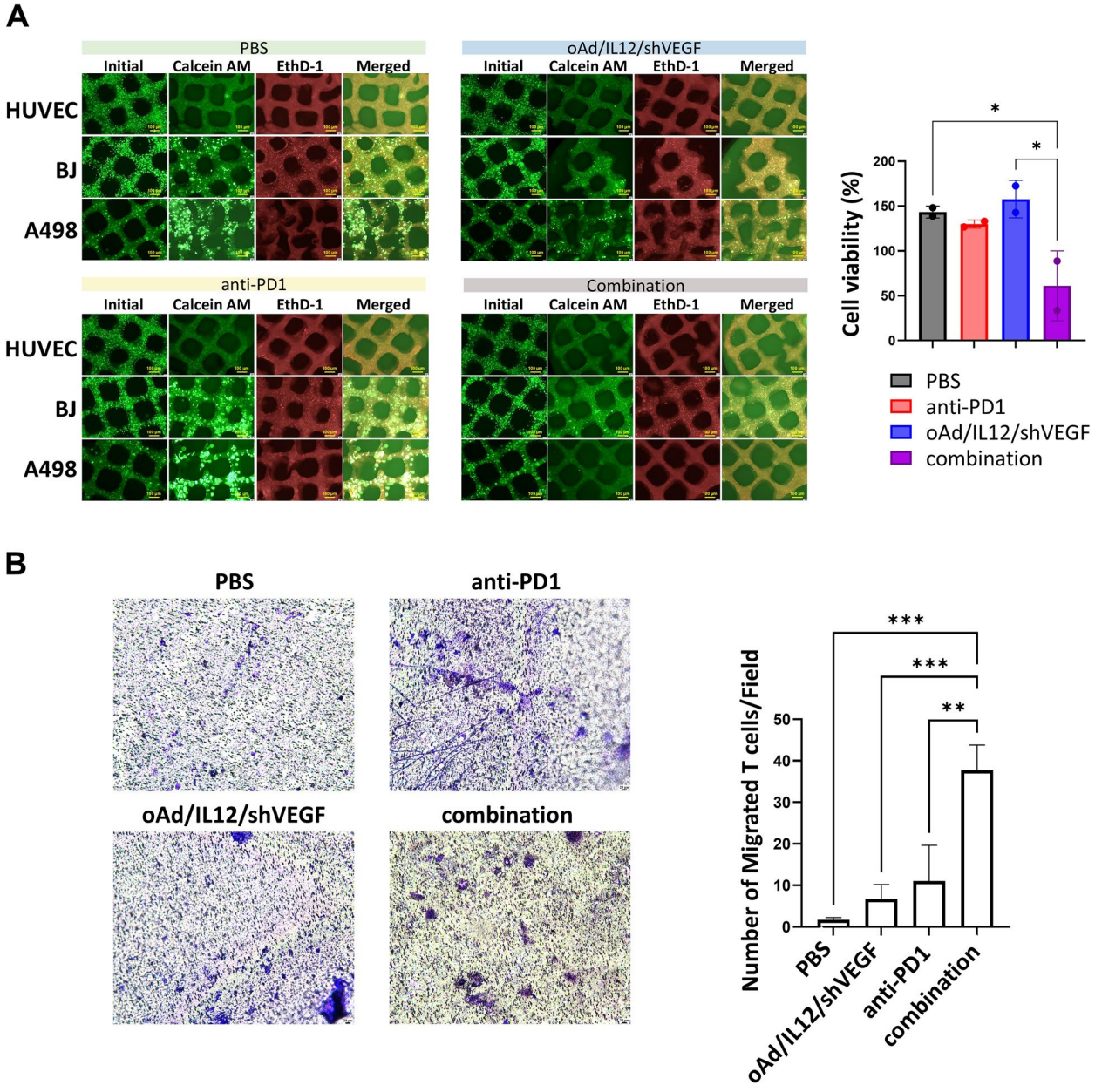

Fig. 4 Potentiated antitumor efficacy and T cell infiltration by combination therapy. **A** Synergistic cancer-killing effect in 3D bioprinted models. Left: Representative fluorescence images (Live/Dead staining) of HUVEC, BJ, and A498 cells following treatment with Control, oAd/IL12/shVEGF 1×10^9 VP), anti-PD1, or the Combination. Right: Quantitative analysis of cell viability at 3 days post-treatment. **B** Evaluation of cellular migration. Left: Representative images of the migration assay (50 × and 100 × magnification) for each treatment group. Right: Quantification of the migration rate based on the migrated area. Data is presented as mean ± SD

revealed no significant pathological alterations on day 15. These results indicate that the oAd-mediated immunotherapy is effective for the treatment of orthotopic RCC with minimal toxicity.

oAd/IL12/shVEGF + anti-PD1 suppresses proliferation and angiogenesis while inducing apoptosis in RCC

To evaluate the therapeutic effect of combination treatment regimen, histological and immunohistochemical analyses of tumor tissues have been performed. As shown in Fig. 6A**,** Hematoxylin and eosin (H & E) and proliferating cell nuclear antigen (PCNA) staining revealed that tumors treated with oAd/IL12/shVEGF + anti-PD1 were nearly devoid of PCNA-positive cell population (* $P < 0.05$, ** $P < 0.01$, *** $P < 0.001$) and that most of the tumor tissues were necrotic. In line with these results, TUNEL staining revealed that oAd/IL12/shVEGF + anti-PD1-treated tumors tissues exhibited highest level

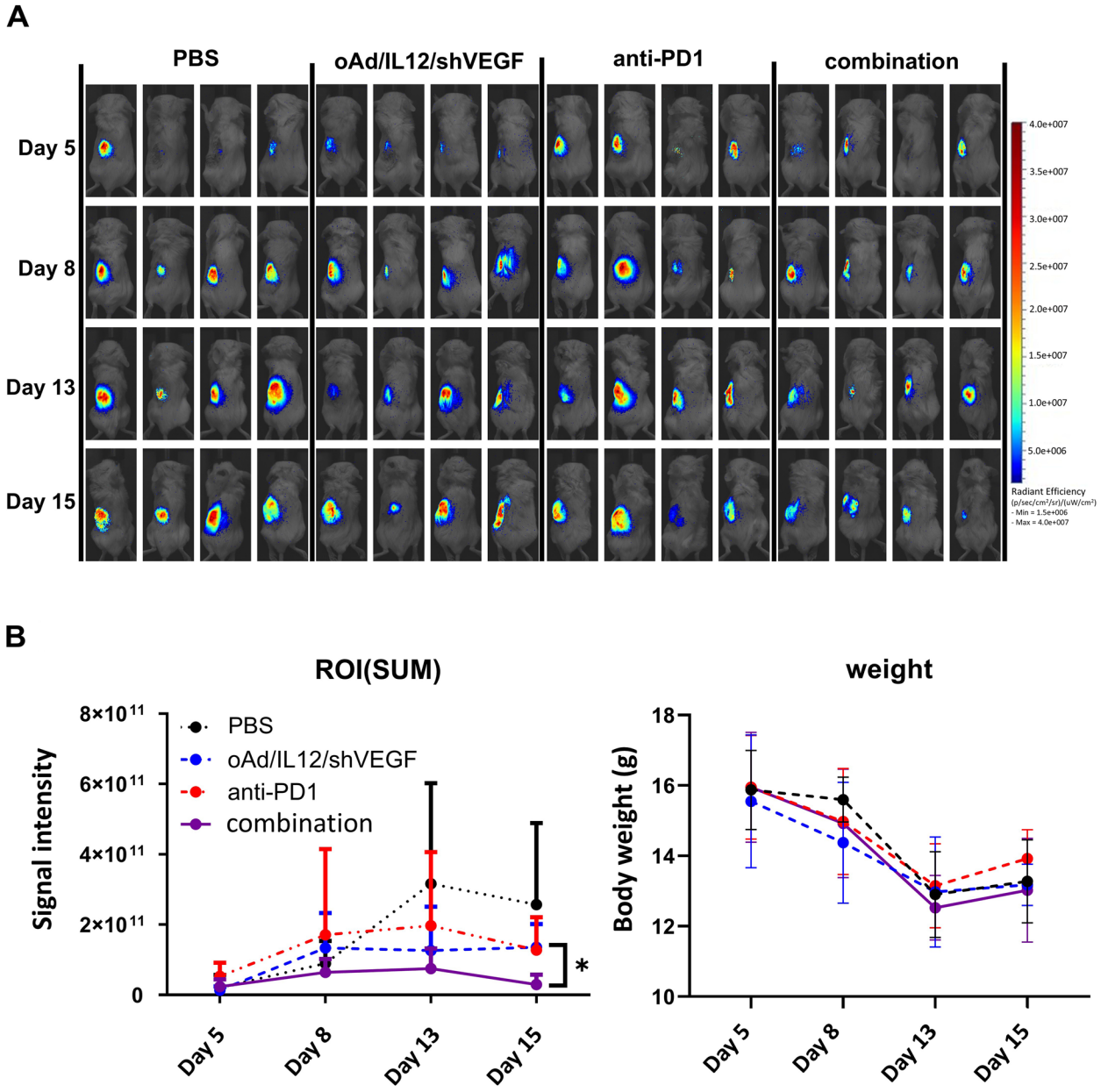

Fig. 5 Potentiated antitumor efficacy of oAd/IL12/shVEGF and anti-PD1 combination in a Renca-luc orthotopic RCC model. **A** Representative bioluminescence images (BLI) of BALB/c mice from each treatment group (PBS, oAd/IL12/shVEGF, anti-PD1, and Combination) at days 5, 8, 10, and 15 post-tumor implantations. Luciferase signals were captured using the IVIS Spectrum system following intraperitoneal administration of D-luciferin (150 mg/kg). **B** Left: Quantitative summary of the total flux (photons/sec) representing tumor burden over time. Right: Changes in body weight of mice across the experimental groups. Data is presented as mean ± SD

of apoptotic cell death over monotherapy options (***$P < 0.001$). These results suggested that combination of oAd/IL12/shVEGF + anti-PD1 effectively induced apoptosis and inhibited proliferation of tumor cells in a synergistic manner. The analysis of tumor infiltrating lymphocyte (TIL) population also revealed that $CD4^+$, $CD8^+$ T and NK cell accumulation was significantly elevated in tumor tissues after treatment with oAd/IL12/shVEGF monotherapy or its combination with anti-PD1 in comparison with PBS control group with extremely low level T cell infiltration (less than 5% of total tumor cell population was either $CD4^+$ and $CD8^+$ T cells; *** $P < 0.001$; Fig. 6B). The oAd/IL12/shVEGF + anti-PD1 induced highest level of $CD4^+$ and $CD8^+$ T cell recruitment in the tumor (* $P < 0.05$ or *** $P < 0.001$ versus oAd/IL12/shVEGF or anti-PD1 monotherapy). These results suggested that the combination therapy induced potent antitumor effect through robust initiation of T cell- or NK-cell mediated antitumor immune response. To further assess oAd/IL12/shVEGF-mediated anti-angiogenic

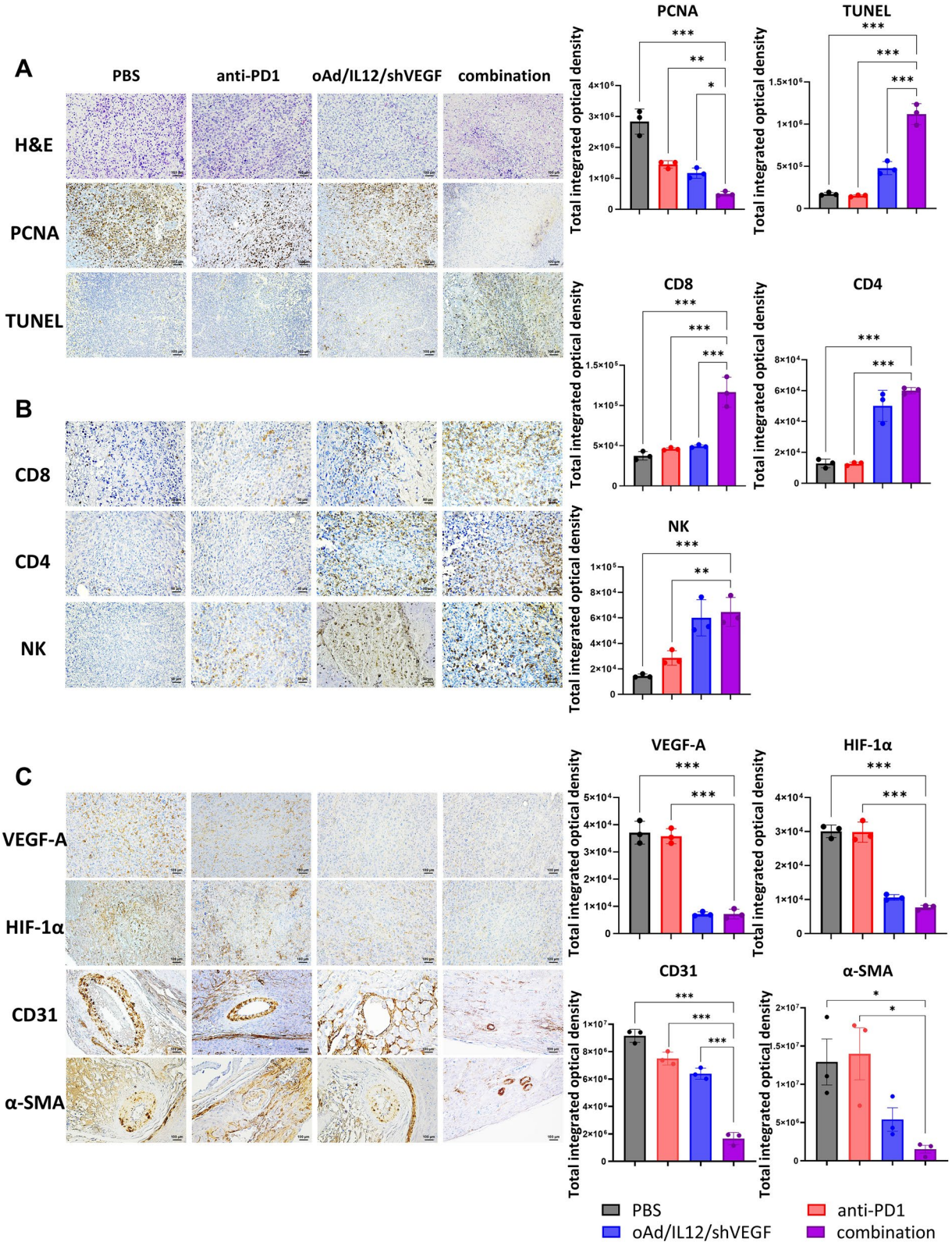

Fig. 6 (See legend on next page.)

(See figure on previous page.)

Fig. 6 Combination therapy remodels the tumor microenvironment by reducing proliferation/hypoxia/angiogenesis and increasing immune infiltration and apoptosis. Tumors from mice treated with PBS, anti-PD1, oAd/IL12/shVEGF, or the combination were collected and analyzed using formalin-fixed, paraffin-embedded (FFPE) sections. **A** Representative images are shown for H&E, PCNA immunohistochemistry (IHC), and TUNEL staining (200×), **B** as well as IHC for CD8, CD4, and NK cell infiltration (400×), and for (**C**) VEGF-A, HIF-1α, CD31, and αSMA (200×). Quantification of indicated markers was performed in ImageJ and expressed as total integrated optical density (IOD). For each tumor, 3 fields were analyzed: $n = 3$ mice/group. Data are presented as mean ± SD. Statistical significance was determined by one-way ANOVA followed by Tukey's multiple-comparisons test; * $P < 0.05$, ** $P < 0.01$, *** $P < 0.001$

effects in the tumor microenvironment, staining for VEGF-A, HIF-1α, CD31, and α-SMA were carried out (Fig. 6C). The expression of VEGF-A and HIF-1α were significantly decreased in oAd/IL12/shVEGF- or oAd/IL12/shVEGF + anti-PD1-treated group compared to the PBS or anti-PD1-treated group shVEGF-mediated mitigation of tumor hypoxia. Furthermore, the decrease in CD31 and α-SMA staining suggests that the combination of oAd/IL12/shVEGF and anti-PD1 effectively inhibits tumor-associated neovascularization.

oAd/IL12/shVEGF + anti-PD1 promotes T cell activation in spleen tissues

To investigate the mechanism behind the antitumor immune response mediated by oAd/IL12/shVEGF + anti-PD1, the splenic $CD4^+$ and $CD8^+$ T cell populations were analyzed. As shown in Fig. 7A, the proportions of $IFN\gamma^+$ or $TNF\alpha^+$ cells among $CD4^+$ and $CD8^+$ T cell populations were slightly increased by anti-PD1 or oAd/IL12/shVEGF monotherapy in comparison with PBS control group In contrast, combination of oAd/IL12/shVEGF with anti-PD1 significantly enhanced the effector functions of both CD4 + and CD8 + T cells in comparison with PBS or anti-PD1 group, as evidenced by the elevated intracellular expression of IFN-γ and TNF-α (** $P < 0.01$, *** $P < 0.001$), suggesting that the combinational strategy was integral to induction of T cell-mediated antitumor immune response. Of note, oAd/IL12/shVEGF + anti-PD1combination therapy induced higher level of $CD8^+$ T cell activation in the spleen in respect to oAd/IL12/shVEGF (* $P < 0.05$), and the $CD4^+$ T cell activation was similarly high between the two groups, showing that both T cell subsets are activated and contribute to the therapeutic outcome. While oAd/IL12/shVEGF + anti-PD1 increased the $CD8^+$ T cell ($CD69^+CD8^+$) population in the spleen compared with monotherapy (*** $P < 0.001$), activated $CD4^+$ T cell ($CD69^+CD4^+$) population also increased compared with monotherapy (Fig. 7B; *** $P < 0.001$), indicating that combination amplifies the activation of CD4 +, $CD8^+$ T cells in RCC. In contrast, $CD25^+Foxp3^+$ regulatory T cells (Tregs) population in $CD3^+$ cell was markedly reduced by the oAd/IL12/shVEGF + anti-PD1, Combination therapy diminished immunosuppressive cell population, leading to alleviate systemic and tumor associated immunosuppression. These data indicate that oAd/IL12/shVEGF + anti-PD1 exerts superior antitumor efficacy by reprogramming the immune environments via enhanced $CD8^+$ T cell and reduced Treg.

Discussion

It is noteworthy that oAd-mediated cancer therapy already has shown remarkable movement in clinical setting for treatment of urologic oncology. The oAd expressing GMCSF, CG0070, has shown promising clinical outcome for the treatment of BCG-refractory patients with non-muscle invasive bladder cancer in a phase II clinical trial (Packiam et al. 2018; Grandi et al. 2023). This achievement highlights promising feasibility of Ad-mediated gene therapy platform for treatment in this disease area. More focusing to RCC, a phase I clinical trial of Enadenotucirev (ColoAd1), which is chimera of large portion of selected genetic elements from Ad11 prototype and Ad3 generated by directed evolution, included RCC patients and demonstrated tumor trafficking of viruses and increased immune-cell infiltration in cancers in both monotherapy and combinations regimens (Garcia-Carbonero et al. 2017). Despite differences in vector engineering method and injection route, the results from these clinical trials indicated that core attributes of oAd (oncolysis and immune priming) are obviously consistent and further reinforce rationale for applying oAd in urologic oncology including bladder cancer and RCC.

The clinical study with early generation oAds, such as CG0070 and ONCOS-102, provide fundamental proof of concept in cancer gene therapy. However, those first- and second-generation oAds, endowing single therapeutic genes and simple genetic modifications, still have an unmet need in the context of tumor specificity, therapeutic potency, and safety. The next-generation oAd platform co-expressing IL-12 and shVEGF is designed to multi target mechanism through potent oncolysis, robust immunomodulation, and effective vascular suppression within the complex tumor microenvironment. Replacement of endogenous E1A promoter to tumor-selective promoter, we shifted forward from the structural simplicity of previous version of vectors. These advancements result in up to 100-fold increased cancer specificity in both human and murine cell lines (Fig. 2). In addition to tumor-selective promoter, the integration of IL-12 and shVEGF leads to approximately a 300% improvement in overall therapeutic efficacy compared to oAd-GMCSF, the analogue version of ONCOS-102 in RCC tumor model (Fig. 3).

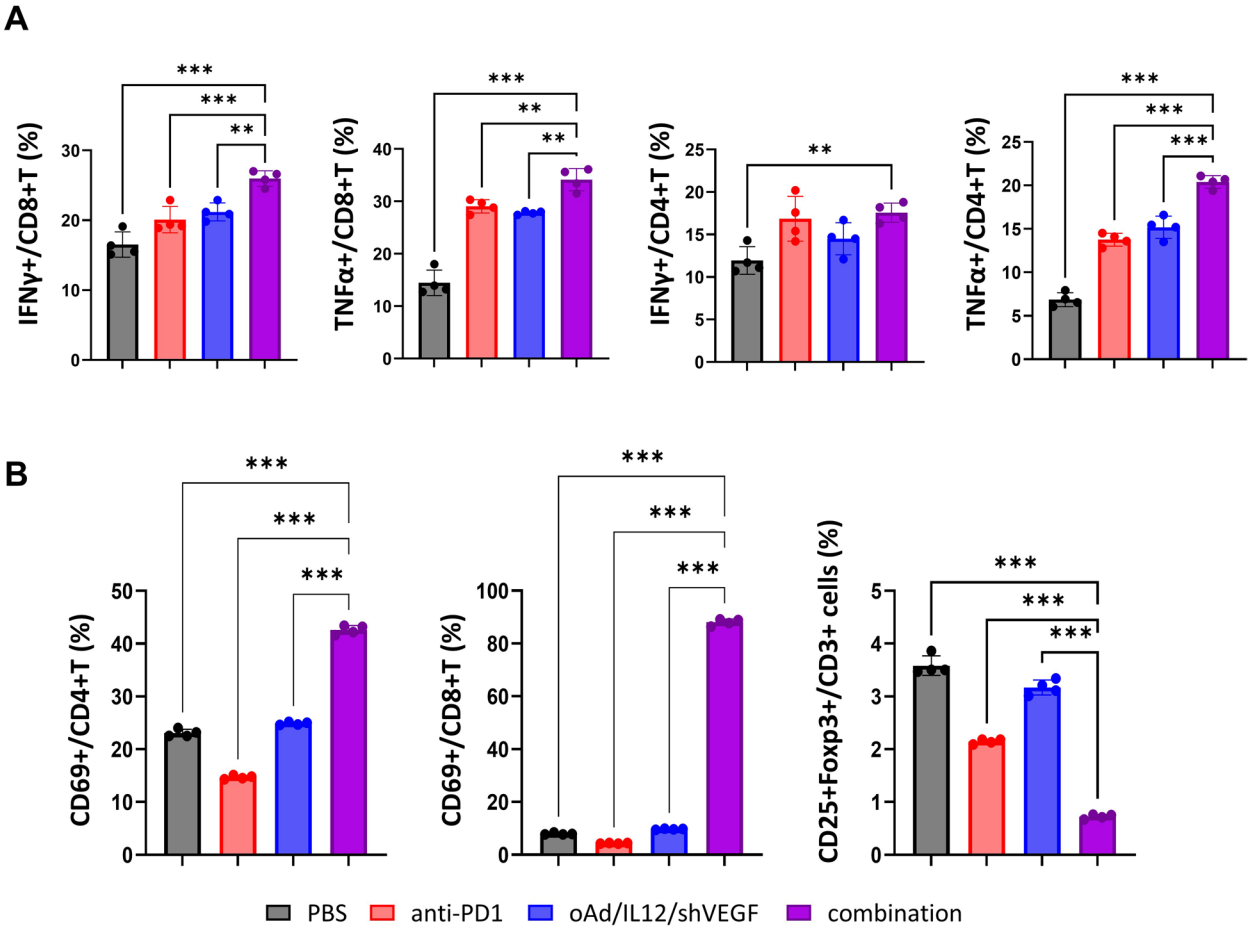

Fig. 7 Combination therapy enhances splenic T-cell effector function and activation while reducing activated Treg frequency. The mice were treated with PBS, anti-PD1, oAd/IL12/shVEGF, or the oAd/IL12/shVEGF + anti-PD1 and splenocytes were analyzed by flow cytometry. For intracellular cytokine staining, cells were stimulated with PMA/ionomycin prior to staining. **A** Frequencies of IFN-γ$^+$ and TNF-α$^+$ cells among CD8$^+$ T cells (top) and CD4$^+$ T cells (bottom). **B** Frequencies of CD69$^+$ cells among CD4$^+$ and CD8$^+$ T cells, and CD25$^+$Foxp3$^+$ cells among CD3.$^+$ T cells. Gates were set using fluorescence-minus-one (FMO) controls. Data are shown as mean ± SD. Statistical significance was assessed by one-way ANOVA followed by Tukey's multiple-comparisons test; * $P < 0.05$, ** $P < 0.01$, *** $P < 0.001$

In this study, we focused on evaluating the therapeutic synergy between our optimized dual-gene platform, oAd/IL12/shVEGF and anti-PD1 blockade, rather than re-evaluating the individual contributions of each transgene. The anti-tumor efficacy of intermediate controls, such as oAd alone, oAd/IL12, and oAd/shVEGF, has been previously established by our group in other tumor models (Xu et al. 2024)**,** demonstrating dual therapeutic gene approach can maximize therapeutic outcomes through simultaneous immune activation and anti-angiogenesis. Based on this rationale, our current work selected the oAd/IL12/shVEGF to explore its potential in overcoming resistance to immune checkpoint inhibitors in the RCC microenvironment. Indeed, these dual therapeutic genes IL12 and shVEGF were selected as therapeutic genes for RCC based on their proven efficacy in simultaneous targeting immunosuppressive and highly angiogenic cancer (Xu et al. 2024; Sorensen et al. 2010). Many clinical and preclinical studies consistently indicate that dual inhibition of these pathways leads to improved therapeutic effects (Xu et al. 2024; Sorensen et al. 2010). Our previous report also demonstrated that oAd-mediated IL12 and VEGF dual targeting strategy maximizes therapeutic efficacy by enhancement of antitumor immune responses and inhibition of angiogenesis (Ahn et al. 2016). Further, there is extensive clinical evidence demonstrating the use of modified IL-12 and VEGF inhibitors for treatments in RCC (Lee et al. 2020; Rini 2007; Dutcher et al. 2020; Strauss et al. 2023; Nadal et al. 2022). Moreover, clinical trials such as KEYNOTE-426 and CheckMate 214 highlighted that combining VEGF receptor inhibitors with immune checkpoint inhibitors results in superior overall survival, progression-free survival, and response rates compared to standard therapies, thereby underscoring the therapeutic benefit of targeting these pathways either

individually or in combination in RCC treatment (Ying et al. 2025; Escudier et al. 2020).

It is worth noting that, beyond its role in immune activation, the murine IL12 expressed by oAd/IL12/shVEGF serves as a powerful anti-angiogenic agent in the human-based 3D model (Figs. 2 and 4) due to its high functional cross-reactivity with human receptors (Gately et al. 1998). The mIL-12-mediated activation of co-cultured T cells and macrophages leads to a robust secretion of IFN-γ, inducing anti-angiogenic effects by promoting the release of CXCL10 and CXCL9. This secondary cytokine signaling effectively targets the HUVEC-based vascular layer, suppressing neovascularization and reducing interstitial pressure even in the absence of shVEGF-mediated silencing. Furthermore, oAd/IL12/shVEGF can demonstrate robust Ad E1A expression and viral replication, as the human RCC A498 is highly permissive host for the Ad5-based oAd. As previously noted, the E1A protein inherently downregulates human VEGF at the transcriptional level, it could provide anti-angiogenic pressure even in the absence of shRNA activity (Yoo et al. 2007). Therefore, combined with IL12-driven anti-angiogenesis, the E1A-mediated transcriptional suppression of VEGF can be a multi-layered attack on the tumor vasculature, providing a consistent therapeutic synergy across different experimental settings.

Pembrolizumab is recommended as representative adjuvant therapy after nephrectomy for patients with high-risk RCC and for metastatic disease, ICI combinations (nivolumab + ipilimumab) or ICI plus tyrosine kinase inhibitors (such as pembrolizumab + axitinib) are standard first-line regimens (Motzer and Bukowski 2006). However, multiple limitations including approximately 80% of non-responders, development of resistance, and inconsistent treatment responses remain in clinical settings (Schmidinger et al. 2025). These non-responders are in 'cold tumor' microenvironment that fail to induce effective antitumor immune responses via insufficient T-cell infiltration, increased presence of immunosuppressive Tregs, and immunosuppressive signals (Wu et al. 2024). Given that combination strategy of oAd/IL12/shVEGF with anti-PD1 may effectively transit tumor microenvironment from a cold to a hot due to marked increase in cytotoxic T-cells infiltration and reduction in Treg in orthotopic tumor (Fig. 6). A central hypothesis regarding the limited efficacy of ICIs in advanced RCC involves the presence of biomechanical and immunological barriers. We propose that the clinical resistance observed in current treatments is fundamentally driven by high interstitial fluid pressure and a 'cold' immune landscape. These factors prevent therapeutic agents and activated T cells from effectively reaching their targets (Jain 2013). Specifically, aberrant VEGF signaling in RCC produces a leaky vasculature that exacerbates intratumoral pressure, creating a physical barrier that blocks drug delivery. Our oAd/IL12/shVEGF virus addresses this by utilizing shVEGF for vascular normalization (Fig. 6C). By stabilizing the microvessel structure and reducing pressure, it facilitates the oncolytic virus and tumor-infiltrating lymphocytes can penetrate better and spread more evenly (Fukumura et al. 2018).

Unlike monotherapy of ICI, oAd replicates directly within the tumor, leading to oncolysis. Further, the danger signals released during this process synergize with the immune-stimulatory effects of IL12, resulting in immune flaming tumor microenvironment (TME) where anti-PD1 can function. In strong agreement with these results, the result from IHC demonstrating infiltration of immune cell into tumors (Fig. 7B), suggesting that oAd/IL12/shVEGF makes the tumor microenvironment more beneficial for recruitment of cytotoxic T cells and NK cells (Fig. 7B). These results address the limitations of current first-line immunotherapies of RCC and provide a promising strategy to broaden their clinical applicability in the treatment.

In conclusion, our current study demonstrates that the next-generation oAd platform, co-expressing IL12 and shVEGF, provides a superior therapeutic strategy for RCC by simultaneously targeting immunosuppressive TME and tumor angiogenesis. By successfully converting 'cold' tumors into 'hot', with increased DC recruitment and CD8 + T-cell infiltration, this platform not only overcomes the limitations of current first-line ICIs but also offers a potent synergistic effect when used in combination with PD1 blockade. These findings suggest that our advanced oAd-mediated cancer gene therapy approach could change the clinical paradigm for treating advanced RCC, particularly for patients who remain refractory to existing immunotherapies. Taking together, these promising preclinical outcomes would guarantee translating into improved survival for patients with urologic malignancies.

Materials and method

Cell lines and culture conditions

Cells were maintained at 37 °C in a humidified incubator with 5% CO_2. Renal cell carcinoma cell lines (Renca-murine cancer cell line; A498, Caki-1, and Caki-2- human cancer cell line), human foreskin fibroblasts (BJ) and mouse embryonic fibroblasts (NIH3T3) were purchased from the American Type Culture Collection (ATCC, Manassas, VA, USA). BJ, NIH3T3, A498, Caki-1, and Caki-2 cells were cultured in Dulbecco's Modified Eagle Medium (DMEM; Gibco) supplemented with 10% fetal bovine serum (FBS; Gibco) and 1% penicillin–streptomycin (P/S; Gibco), whereas Renca cells were maintained in RPMI-1640 medium (Gibco) supplemented with 10% FBS and 1% P/S. Cells were routinely passaged at 70–90%

confluence using standard procedures, and low-passage cells were used for all experiments.

Preparation of oAd/IL12/shVEGF

To produce oAd, oAd/IL12/shVEGF genome containing plasmid was linearized with PacI (New England Biolabs, Ipswich, MA) then transfected into 293 A cells using JetPrime transfection reagent (Polyplus, Illkirch, France) according to manufacturer's instructions. All Ads were propagated in A549 cells and purified by CsCl gradient centrifugation. The number of VP was determined by measuring the optical density at 260 nm, for which an absorbance value of 1 is equivalent to 1.1×10^{12} VP/mL. Purified viruses were stored at −80 °C until use.

Cytokine/angiogenic factor quantification ELISA

For cytokine/angiogenic factor quantification, A498 and Renca cells were seeded in 6-well plates at 2 × 10^5 cells/well and were infected the following day with oAd/IL12/shVEGF at the indicated multiplicities of infection (MOI; A498: 0, 1, 2, 5, 10, and 20; Renca: 0, 5, 10, 20, 50, and 100). At 48 h post-infection, conditioned media were harvested, clarified by centrifugation to remove debris, and used for ELISA-based quantification of secreted IL12 and VEGF-A. IL12 was measured using an IL12 p70 DuoSet ELISA kit (R&D Systems; DY1270), and VEGF-A was measured using a VEGF-A ELISA kit (Thermo Fisher Scientific; BMS277-2), according to the manufacturers' instructions. Concentrations were calculated from standard curves and reported as pg/mL.

Cancer cell killing assay

The cancer cell–specific cytotoxicity of oAd was assessed using an MTT assay based on the conversion of 3-(4,5-dimethylthiazolyl-2)–2,5-diphenyltetrazolium bromide (MTT; Sigma, Livonia, MI, USA) to formazan. Human cell lines (BJ, A498, Caki-1, and Caki-2) and mouse cell lines (NIH3T3 and Renca) were seeded in 96-well plates overnight and then infected with oAd at the indicated multiplicities of infection (MOI; 0.1–1000), with PBS-treated wells included as negative controls. At 48 h post-infection, 50 μL of MTT solution (2 mg/mL in PBS) was added to each well and incubated at 37 °C for 4 h. The supernatant was removed, and the resulting formazan crystals were dissolved in 200 μL of dimethyl sulfoxide (DMSO; Sigma). Absorbance was measured at 540 nm using a microplate reader, and cell viability was calculated by normalizing PBS-treated wells (set to 100%). All conditions were assayed in triplicate, and IC50 values were determined from dose–response curves.

Fabrication of 3D Bioprinted RCC Model

Based on the optimization of the renal cancer microenvironment, a 3D bioprinted lattice model was fabricated to evaluate the efficacy of oAd/IL12/shVEGF. For the 3D scaffold, Gel4Cell (Innoregen, Incheon, Korea), a gelatin methacryloyl (GelMA)-based bio-ink, was utilized as the primary extracellular matrix (ECM) surrogate. The bioprinting process was conducted using an extrusion-based 3D bioprinter (Innoregen). The cell-laden bio-ink, containing a co-culture of A498 cells, BJ, and HUVEC, was extruded through a 27G nozzle at a translation speed of 5 mm/s. To ensure structural stability, the printed lattice constructs were stabilized via photo crosslinking using 405 nm visible light for 90 s. To mimic a physiologically relevant tumor-immune microenvironment, we developed a multi-layered infiltration model using a migration filter. A mixture of Jurkat T cells and THP-1 cells, the latter of which were pre-differentiated into macrophages using phorbol 12-myristate 13-acetate (PMA), was placed in the bottom chamber. The migration filter was then overlaid with successive layers of HUVEC, BJ fibroblasts, and A498 cancer cells. This 3D architecture supported the evaluation of viral penetration, the anti-PD1, and the active infiltration of immune cells through multi-cellular barriers. To assess cell-type specific viability, ROI analysis was performed. Fluorescence signals were quantified specifically within the spatial compartments assigned to A498, BJ, or HUVEC cells during bioprinting using ImageJ software.

Viral infection and drug treatment

The 3D bioprinted constructs were infected with oAd/IL12/shVEGF at concentrations ranging from 1×10^8 to 1×10^{10} VP. For combination studies, anti-PD1 (200 μg/20 g equivalent or optimized concentration) was administered alongside the viral treatment. The therapeutic effects were compared across monotherapy and combination groups to evaluate potential synergistic antitumor activity within the 3D microenvironment. 3.3. Live/Dead Staining and Viability Assay Cell viability within the 3D bioprinted model was assessed at 24 h (1D) and 72 h (3D) after treatment. A live/dead staining kit containing calcein AM (green; live) and ethidium homodimer-1 (red; dead) (Thermo Fisher Scientific) was employed according to the manufacturer's instructions. Fluorescence images were captured using a fluorescence microscope at 50 × magnification. Three independent bioprinted constructs were analyzed for each experimental condition to ensure statistical reliability.

In vitro cytotoxicity and migration assay

The bioprinted constructs integrated with the immune cell infiltration system were infected with oAd/IL12/shVEGF at various concentrations (1×10^8 to 1×10^{10} VP) or treated with anti-PD1 for combination studies. Cell viability was assessed at 1 and 3 days post-treatment using a Live/Dead assay (Calcein AM for live cells;

Ethidium homodimer-1 for dead cells). For the anti-tumor migration efficacy (Fig. 4B), the recruitment of immune cells from the bottom chamber toward the top tumor-cell layers was evaluated. The number of Jurkat T cells and differentiated THP-1 cells that successfully infiltrated through the filter and the vascular/fibroblast layers were quantified using ImageJ software. This allowed for the assessment of the synergistic effect of the combination therapy on enhancing the chemotactic recruitment of immune cells into the dense 3D tumor mass.

Orthotopic renal cell carcinoma mouse model and treatment

Six-week-old female BALB/c mice (Orient Bio Co., Seongnam, Korea) were acclimated for 1 week under standard laboratory conditions before the experiments. To establish the orthotopic RCC model, Renca-luciferase (Renca-luc) cells were prepared in serum-free medium at a concentration of 5×10^5 cells/50 µL. Mice were anesthetized with isoflurane, and the right kidney was exposed through a small flank incision. Using a 30-gauge needle, the tumor cells were precisely injected into the subcapsular space of the kidney, and the incision was closed with absorbable sutures. For the anti-PD1 group, 200 µg of anti-PD1 antibody was administered via intraperitoneal (IP) injection a total of four times on days 1, 4, 8, and 11. For the OV group, oAd/IL12/shVEGF (1×10^9 VP in 50 µL PBS) was injected intraperitoneally on days 2, 5, 9, and 12. The combination group received both agents following the same respective schedules, while control mice received an equal volume of PBS. Tumor progression was monitored via bioluminescence imaging (BLI) using an IVIS Spectrum in vivo imaging system (PerkinElmer, Waltham, MA, USA) at days 5, 8, 13, and 15 post-implantations. On day 18, all mice were sacrificed for further analysis.

Subcutaneous renal cell carcinoma mouse model and anti-tumor effects

To establish subcutaneous tumor models, Renca 5×10^5 cells/animal) or A498 (3×10^6 cells/animal) cells were subcutaneously (s.c.) injected into the right flank of mice. When tumors reached a 100 mm^3, mice were randomized into treatment groups. For the treatment of Renca tumors, PBS or oAd/IL12/shVEGF (1×10^8 VP) was administered via three intratumoral (i.t.) injections, with or without concurrent intraperitoneal (i.p.) administration of anti-PD1 antibody (200µg/dose). For the A498 xenograft model, a dose-escalation study was performed where mice received three i.t. injections of PBS or oAd/IL12/shVEGF at doses of 1×10^6, 1×10^7, 1×10^8 VP. In both models, tumor growth was monitored every 7 days, and tumor volumes were calculated using the formula: Tumor volume = $0.523 \times L \times w^2$.

Animal care

All animal experiments were performed in accordance with the Institutional Animal Care and Use Committee (IACUC) guidelines and regulations of Hanyang University and Chung-Ang University, and were approved by the Hanyang University IACUC (approval numbers: HYU-2024-0278A and HYU-2025-0025A; Chung-Ang University approval number: A2021020). Female BALB/c and BALB/c nude mice were purchased from Orient Bio (Seongnam, Republic of Korea). Mice were weighed, caged, housed, and maintained under standard specific pathogen–free (SPF) conditions with a 12 h light/dark cycle.

Flow cytometry

Single-cell suspensions of splenocytes were prepared from the harvested spleens of BALB/c mice. Briefly, the spleens were placed in cold PBS and mechanically dissociated through a 70 µm nylon cell strainer (BD Biosciences). The cell suspension was centrifuged at 300 X g for 10 min at 4 °C. To eliminate red blood cells, the resulting pellet was resuspended in 10 mL of 1 × RBC Lysis Buffer (diluted from 10 × stock; BioLegend, San Diego, CA, USA) and incubated for 10 min on ice. The lysis reaction was immediately quenched by adding 10 mL of complete medium. After an additional centrifugation step, the splenocytes were resuspended in fresh medium and filtered once more to ensure a debris-free population. The cell concentration and viability were determined using a hemocytometer with Trypan blue exclusion, and only samples with > 95% viability were utilized for subsequent assays. Flow cytometry was performed in two independent experiments using two antibody panels (Panel 1: Treg/activation; Panel 2: cytokine). Single-cell suspensions were prepared from the indicated samples, washed, and stained with Live/Dead Fixable Yellow (Invitrogen; L34959) according to the manufacturer's instructions, followed by surface staining with fluorochrome-conjugated antibodies in staining buffer. For Panel 1, cells were stained for CD45 (BV711; clone I3/2.3; BD; 752408), CD3 (FITC; clone 17A2; BD; 561798), CD4 (BV786; clone GK1.5; BD; 563331), CD8 (PerCP-Cy5.5; clone 53–6.7; BD; 551162), CD25 (PE-Cy7; clone 3C7; BioLegend; 101916), and CD69 (PE; clone H1.2F3; BioLegend; 104507), followed by intracellular staining for Foxp3 (Alexa Fluor 647; clone MF23; BD; 560401) after fixation/permeabilization using a standard Foxp3 staining workflow. For Panel 2, cells were stained for CD45 (BV711; clone I3/2.3; BD; 752408), CD3 (FITC; clone 17A2; BD; 561798), CD4 (BV786; clone GK1.5; BD; 563331), and CD8 (PerCP-Cy5.5; clone 53–6.7; BD; 551162), followed by intracellular staining for IFN-γ (eFluor 450; clone XMG1.2; Invitrogen; 48–7311-82) and TNF-α (PE; clone MP6-XT22; R&D Systems; IC410P) after

fixation/permeabilization. After final washes, samples were acquired on a BD FACSymphony A3 (BD Biosciences) at the Hanyang University Core Facility (Seoul, Korea) equipped with 405/488/561/640 nm lasers (detectors 431/28, 515/20, 586/15, 670/30, 710/50, 780/60). Compensation was set up using single-stained controls, with FMO controls for cytokine gates. Data was analyzed in FlowJo software (BD) with the gating sequence: singlets → live cells → $CD45^+$ lymphocytes → $CD3^+$ T cells → $CD4^+$ or $CD8^+$ subsets → IFN-γ^+, TNF-α^+, and frequencies reported as % of the parent population All stains were performed in technical duplicates and repeated in at least two independent experiments.

Immunohistochemical and histological analysis

Tumors were harvested from Renca tumor–bearing mice at 3 days after the final intratumoral virus administration and immediately fixed in 4% paraformaldehyde (PFA). Paraffin embedding, sectioning, hematoxylin and eosin (H&E) staining were performed by K2O (Republic of Korea), and paraffin sections were prepared at a thickness of 5 μm. For immunohistochemistry (IHC), sections were deparaffinized and rehydrated using standard procedures, blocked with Protein Block Serum-Free solution (Agilent Technologies, Santa Clara, CA, USA) for 30 min at room temperature, and incubated overnight at 4 °C with primary antibodies against CD4 (clone 4SM95, Invitrogen; 1:200), CD8a (clone 4SM15, Invitrogen; 1:200), NKp46/CD335 (clone 29A1.4, Thermo Fisher Scientific), PCNA (clone PC10, Santa Cruz Biotechnology), VEGF-A (ab1316, Abcam), HIF-1α (clone D1S7W, Cell Signaling Technology; #36169), CD31/PECAM-1 (clone 390, Thermo Fisher Scientific), or αSMA (ab5694, Abcam). After washing, signal detection was performed using the Dako REAL EnVision Detection System (Rabbit/Mouse; Agilent/Dako), and chromogenic visualization was carried out with 3,3′-diaminobenzidine (DAB) using the Dako Liquid DAB + Substrate Chromogen System (K5007; Agilent/Dako), according to the manufacturer's instructions. Apoptotic cell death was evaluated by terminal deoxynucleotidyl transferase dUTP nick end labeling (TUNEL) staining using the DeadEnd Colorimetric TUNEL System (Promega) according to the manufacturer's protocol. Images were acquired using a light microscope (Eclipse Ci, Nikon).

Statistical analysis

The data are presented as mean of SEM and SD. Statistical analyses were performed using GraphPad PRISM ver. 8.3 (GraphPad Software, Boston, MA). A two-tailed Student's t-test and one-way ANOVA (Tukey multiple comparison test) were used. $^*P < 0.05$; $^{**}P < 0.01$, $^{***}P < 0.001$, n.s; not significant.

Supplementary Information

The online version contains supplementary material available at https://doi.org/10.1186/s10020-026-01535-z.

Supplementary Material 1.

Acknowledgements

The research was supported by a grant of Korea Health Technology R&D Project through the Korea Health Industry Development Institute (KHIDI), funded by the Ministry of Health & Welfare (RS-2024-00439816, C-O. Y.; RS-2025-02263117, A-R. Y.), Ministry of Food and Drug Safety, Republic of Korea (RS-2024-00395863, A-R. Y.), National Research Foundation of Korea (2023R1A2C1003830, S. C.; RS-2024-00342763; J. C.) and Korea Basic Science Institute (National research Facilities and Equipment Center) grant funded by the Ministry of Education (2023R1A6C101A009).

Declaration of AI and AI-assisted technologies in the writing process

During the preparation of this work, the authors used ChatGPT, based on GPT-4/5 (OpenAI, San Francisco, CA) and Grammarly (San Francisco, CA) to improve the language and readability. After using this tool, the authors reviewed and edited the content as needed and took full responsibility for the content of the publication.

Authors' contributions

Conceptualization, I-H. J.; C-O. Y. writing-original draft preparation, J. C.; S-M.; A-R. Y. revision experiment, E. P. writing-review and editing, I-H. J.; C-O. Y. A-R. Y. Funding acquisition, C-O. Y. A-R. Y. Proofreading, J. C.; S-M.; A-R. Y. Experimental work, J. Y.; Y. K.; S-M. Data analysis, J. Y.;Y. K.; S-M.

Funding

The research was supported by a grant of Korea Health Technology R&D Project through the Korea Health Industry Development Institute (KHIDI), funded by the Ministry of Health & Welfare (RS-2024–00439816, C-O. Y.; RS-2025–02263117, A-R. Y.), National Research Foundation of Korea (2023R1A2C1003830, S. C.; RS-2024–00342763, J. C.) and Korea Basic Science Institute (National research Facilities and Equipment Center) grant funded by the Ministry of Education (2023R1A6C101A009).

Data availability

All data relevant to the study are included in the article or uploaded as supplementary information.

Declarations

Ethics approval and consent to participate

This study is reported in accordance with the ARRIVE guidelines. All animal experiments were approved by the Institutional Animal Care and Use Committee (IACUC) (Hanyang University: HYU-2025-0025A HYU-2024-0278A and HYU-2025-0025A; Chung-Ang University approval number: A2021020) and conduct in accordance with relevant guidelines and regulations. No human participants were involved in this study. For institutional research integrity/ethics inquiries, please contact: irb@hanyang.ac.kr (Institutional Review Board/Research Ethics Office, Hanyang University).

Competing interests

The authors declare no competing interests.

Author details

[1]Department of Urology, Chung-Ang University Gwangmyeong Hospital, Chung-Ang University College of Medicine, Gwangmyeong, South Korea
[2]Department of Bioengineering, College of Engineering, Hanyang University, Seoul, South Korea
[3]Institute of Nano Science and Technology (INST), Hanyang University, Seoul, South Korea
[4]Hanyang Institute of Bioscience and Biotechnology (HY-IBB), Hanyang University, Seoul, South Korea
[5]GeneMedicine CO., Ltd., Seoul 04763, South Korea
[6]Department of Urology, Chung-Ang University Hospital, Chung-Ang University College of Medicine, Seoul, South Korea

[7]Asan Institute for Life Sciences, Asan Medical Center, Seoul, South Korea
[8]Department of Urology, Asan Medical Center, University of Ulsan College of Medicine, Seoul, Korea

Received: 6 March 2026 / Accepted: 16 June 2026
Published online: 26 June 2026

References

Ahn HM, Hong J, Yun CO. Oncolytic adenovirus coexpressing interleukin-12 and shVEGF restores antitumor immune function and enhances antitumor efficacy. Oncotarget. 2016;7(51):84965–80. https://doi.org/10.18632/oncotarget.13087. PubMed PMID: 27821803; PubMed Central PMCID: PMCPMC5356712.

Ahn HM, Jung BK, Hong J, Hong D, Yoon AR, Yun CO. Enhanced potency of immune checkpoint inhibitors against poorly immunological solid tumors by immune stimulatory oncolytic adenoviruses-mediated remodeling of the tumor microenvironment. Mol Med. 2025;31(1):175. https://doi.org/10.1186/s10020-025-01223-4. PubMed PMID: 40335925; PubMed Central PMCID: PMCPMC12057182. Epub 20250507.

Amin A, Hammers H. The evolving landscape of immunotherapy-based combinations for frontline treatment of advanced renal cell carcinoma. Front Immunol. 2018;9:3120. https://doi.org/10.3389/fimmu.2018.03120.

Bedke J, Albiges L, Capitanio U, Giles RH, Hora M, Ljungberg B, et al. The 2022 updated European association of urology guidelines on the use of adjuvant immune checkpoint inhibitor therapy for renal cell carcinoma. Eur Urol. 2022;83(1):10–4. https://doi.org/10.1016/j.eururo.2022.10.010.

Cheng C, Wang Q, Zhang S. Synergy of oncolytic adenovirus and immune checkpoint inhibitors: transforming cancer immunotherapy paradigms. Front Immunol. 2025;16:1610858. https://doi.org/10.3389/fimmu.2025.1610858.

Choi SY, Kim M, Kang SJ, Choi YW, Maeng S, Kim S-H, et al. Enhanced antitumor effect of the combination of Bacille Calmette-Guérin and an immune checkpoint inhibitor in bladder cancer-on-a-chip. BioChip J. 2023;17(4):496–506. https://doi.org/10.1007/s13206-023-00125-z.

Coppin C, Porzsolt F, Awa A, Kumpf J, Coldman A, Wilt T. Immunotherapy for advanced renal cell cancer. Cochrane Database Syst Rev. 2005;(1):CD001425. Epub 20050125. https://doi.org/10.1002/14651858.CD001425.pub2. PubMed PMID: 15674877.

Dutcher JP, Flippot R, Fallah J, Escudier B. On the shoulders of giants: the evolution of renal cell carcinoma treatment-cytokines, targeted therapy, and immunotherapy. Am Soc Clin Oncol Educ Book. 2020;40:1–18. https://doi.org/10.1200/edbk_280817. PubMed PMID: 32243201.

Escudier B, Motzer RJ, Tannir NM, Porta C, Tomita Y, Maurer MA, et al. Efficacy of Nivolumab plus Ipilimumab according to number of IMDC risk factors in CheckMate 214. Eur Urol. 2020;77(4):449–53. https://doi.org/10.1016/j.eururo.2019.10.025.

Fukumura D, Kloepper J, Amoozgar Z, Duda DG, Jain RK. Enhancing cancer immunotherapy using antiangiogenics: opportunities and challenges. Nat Rev Clin Oncol. 2018;15(5):325–40. https://doi.org/10.1038/nrclinonc.2018.29.

Garcia-Carbonero R, Salazar R, Duran I, Osman-Garcia I, Paz-Ares L, Bozada JM, et al. Phase 1 study of intravenous administration of the chimeric adenovirus enadenotucirev in patients undergoing primary tumor resection. J Immunother Cancer. 2017;5(1):71. https://doi.org/10.1186/s40425-017-0277-7.

Gately MK, Renzetti LM, Magram J, Stern AS, Adorini L, Gubler U, et al. The interleukin-12/interleukin-12-receptor system: role in normal and pathologic immune responses. Annu Rev Immunol. 1998;16:495–521. https://doi.org/10.1146/annurev.immunol.16.1.495. PubMed PMID: 9597139.

Grandi P, Darilek A, Moscu A, Pradhan A, Li R. Intravesical infusion of oncolytic virus CG0070 in the treatment of bladder cancer. Methods Mol Biol. 2023;2684:303–17. https://doi.org/10.1007/978-1-0716-3291-8_19. PubMed PMID: 37410243.

Jain RK. Normalizing tumor microenvironment to treat cancer: bench to bedside to biomarkers. J Clin Oncol. 2013;31(17):2205–18. https://doi.org/10.1200/jco.2012.46.3653. PubMed PMID: 23669226; PubMed Central PMCID: PMCPMC3731977. Epub 20130513.

Jian Y, Yang K, Sun X, Zhao J, Huang K, Aldanakh A, et al. Current advance of immune evasion mechanisms and emerging immunotherapies in renal cell carcinoma. Front Immunol. 2021;12:639636. https://doi.org/10.3389/fimmu.2021.639636.

Lee WS, Yang H, Chon HJ, Kim C. Combination of anti-angiogenic therapy and immune checkpoint blockade normalizes vascular-immune crosstalk to potentiate cancer immunity. Exp Mol Med. 2020;52(9):1475–85. https://doi.org/10.1038/s12276-020-00500-y.

Liu L, Song L, Liu T, Hui K, Hu C, Yang J, et al. Recombinant oncolytic virus NDV-anti-VEGFR2 enhances radiotherapy sensitivity in NSCLC by targeting VEGF signaling and impairing DNA repair. Gene Ther. 2025;32:517. https://doi.org/10.1038/s41434-025-00540-x. PubMed PMID: 40382521. Epub 20250517.

Liu W, Cao Y, Fernandez MI, Niu H, Xiu Y. Additive antitumoral effect of interleukin-12 gene therapy and chemotherapy in the treatment of urothelial bladder cancer in vitro and in vivo. Int Urol Nephrol. 2011;43(3):721–7. https://doi.org/10.1007/s11255-010-9866-9.

Logan JE, Rampersaud EN, Sonn GA, Chamie K, Belldegrun AS, Pantuck AJ, et al. Systemic therapy for metastatic renal cell carcinoma: a review and update. Rev Urol. 2012;14(34):65–78. PubMed PMID: 23526579; PubMed Central PMCID: PMCPMC3602729.

Motzer RJ, Bukowski RM. Targeted therapy for metastatic renal cell carcinoma. J Clin Oncol. 2006;24(35):5601–8. https://doi.org/10.1200/JCO.2006.08.5415. PubMed PMID: 17158546.

Motzer RJ, Hutson TE, Tomczak P, Michaelson MD, Bukowski RM, Rixe O, et al. Sunitinib versus interferon alfa in metastatic renal-cell carcinoma. N Engl J Med. 2007;356(2):115–24. https://doi.org/10.1056/NEJMoa065044. PubMed PMID: 17215529.

Nadal L, Peissert F, Elsayed A, Weiss T, Look T, Weller M, et al. Generation and in vivo validation of an IL-12 fusion protein based on a novel anti-human FAP monoclonal antibody. J Immunother Cancer. 2022;10(9):e005282. https://doi.org/10.1136/jitc-2022-005282. PubMed PMID: 36104101; PubMed Central PMCID: PMCPMC9476130.

Packiam VT, Lamm DL, Barocas DA, Trainer A, Fand B, Davis RL, et al. An open label, single-arm, phase II multicenter study of the safety and efficacy of CG0070 oncolytic vector regimen in patients with BCG-unresponsive non-muscle-invasive bladder cancer: interim results. Urol Oncol. 2018;36(10):440–7. https://doi.org/10.1016/j.urolonc.2017.07.005.

Qian X, Ning W, Yang J, Dunmall LC, Pandha HS, Shang G, et al. The oncolytic adenovirus Ad-TD-nsIL12 in primary or progressive pediatric IDH wild-type diffuse intrinsic pontine glioma results of two phase I clinical trials. Nat Commun. 2025;16(1):6934. https://doi.org/10.1038/s41467-025-62260-5.

Rini BI. Vascular endothelial growth factor-targeted therapy in renal cell carcinoma: current status and future directions. Clin Cancer Res. 2007;13(4):1098–106. https://doi.org/10.1158/1078-0432.Ccr-06-1989. PubMed PMID: 17317817.

Schmidinger M, Rane PP, Yan K, Druyts E, Burgents J, Sundaram M, et al. Efficacy of first-line treatments for advanced renal cell carcinoma: a Bayesian network meta-analysis of objective response, progression-free survival, and overall survival. Target Oncol. 2025;20(3):375–87. https://doi.org/10.1007/s11523-025-01147-3.

Sorensen EW, Gerber SA, Frelinger JG, Lord EM. IL-12 suppresses vascular endothelial growth factor receptor 3 expression on tumor vessels by two distinct IFN-gamma-dependent mechanisms. J Immunol. 2010;184(4):1858–66. https://doi.org/10.4049/jimmunol.0903210. PubMed PMID: 20061409; PubMed Central PMCID: PMCPMC3070472. Epub 20100108.

Strauss J, Deville JL, Sznol M, Ravaud A, Maruzzo M, Pachynski RK, et al. First-in-human phase Ib trial of M9241 (NHS-IL12) plus avelumab in patients with advanced solid tumors, including dose expansion in patients with advanced urothelial carcinoma. J Immunother Cancer. 2023;11(5):e005813. https://doi.org/10.1136/jitc-2022-005813. PubMed PMID: 37236636; PubMed Central PMCID: PMCPMC10230972.

Wolf MM, Rathmell WK, de Cubas AA. Immunogenicity in renal cell carcinoma: shifting focus to alternative sources of tumour-specific antigens. Nat Rev Nephrol. 2023;19(7):440–50. https://doi.org/10.1038/s41581-023-00700-5. PubMed PMID: 36973495; PubMed Central PMCID: PMCPMC10801831. Epub 20230327.

Wu B, Zhang B, Li B, Wu H, Jiang M. Cold and hot tumors: from molecular mechanisms to targeted therapy. Signal Transduct Target Ther. 2024;9(1):274. https://doi.org/10.1038/s41392-024-01979-x.

Xu Y, Sun X, Tong Y. Interleukin-12 in multimodal tumor therapies for induction of anti-tumor immunity. Discov Oncol. 2024;15(1):170. https://doi.org/10.1007/s12672-024-01011-2.

Yang M, Mu Y, Yu X, Gao D, Zhang W, Li Y, et al. Survival strategies: how tumor hypoxia microenvironment orchestrates angiogenesis. Biomed Pharmacother. 2024;176:116783. https://doi.org/10.1016/j.biopha.2024.116783.

Ying H, Tong F, Zhou Y, Zhou B, Qiao K, Chen L, et al. A cost-effectiveness comparison between immunotherapy combination regimens and sunitinib for advanced renal cell carcinoma in the USA and China. Ther Adv Med Oncol. 2025;17:17588359251385392. https://doi.org/10.1177/17588359251385392.

Yoo JY, Kim JH, Kwon YG, Kim EC, Kim NK, Choi HJ, et al. VEGF-specific short hairpin RNA-expressing oncolytic adenovirus elicits potent inhibition of angiogenesis and tumor growth. Mol Ther. 2007;15(2):295–302. https://doi.org/10.1038/sj.mt.6300023. PubMed PMID: 17235307.

Yoon AR, Hong J, Jung BK, Ahn HM, Zhang S, Yun CO. Oncolytic adenovirus as pancreatic cancer-targeted therapy: where do we go from here? Cancer Lett. 2023;579:216456. https://doi.org/10.1016/j.canlet.2023.216456.

Yoon AR, Hong J, Li Y, Shin HC, Lee H, Kim HS, et al. Mesenchymal Stem Cell-Mediated delivery of an oncolytic adenovirus enhances antitumor efficacy in hepatocellular carcinoma. Cancer Res. 2019;79(17):4503–14. https://doi.org/10.1158/0008-5472.CAN-18-3900.

Young M, Jackson-Spence F, Beltran L, Day E, Suarez C, Bex A, et al. Renal cell carcinoma. Lancet. 2024;404(10451):476–91. https://doi.org/10.1016/S0140-6736(24)00917-6.

Publisher's Note

Springer Nature remains neutral with regard to jurisdictional claims in published maps and institutional affiliations.